Probing the extended-state width of disorder-broadened Landau levels in epitaxial graphene

K. Takase,[*] H. Hibino,[†] and K. Muraki

NTT Basic Research Laboratories, NTT Corporation, 3-1 Morinosato-Wakamiya, Atsugi, Kanagawa 243-0198, Japan
(Received 31 July 2013; revised manuscript received 2 June 2015; published 8 September 2015)

We experimentally investigate the width of extended states in disorder-broadened Landau levels (LLs) in top-gated epitaxial graphene on silicon carbide using two different methods: gated transport spectroscopy and activation gap measurements on integer quantum Hall states. The transport spectroscopy reveals that the widths of the extended states in the zero-energy ($N = 0$) and first excited ($N = 1$) LLs are of similar magnitude over the ranges of magnetic field (4–16 T) and temperature studied (1.6–150 K). Under certain assumptions we find that the extended-state width follows a power-law temperature dependence with the exponent $\eta \sim 0.3$ in the $N = 0$ ($N = 1$) LL, with almost no (very weak) magnetic-field dependence. Activation gap measurements at the filling factors of $\nu = 2$ and 6 give results consistent with transport spectroscopy for the $N = 1$ LL, but indicate a larger broadening for the $N = 0$ LL than deduced from the spectroscopy.

I. INTRODUCTION

Graphene, a single layer of carbon atoms arranged in a honeycomb lattice, possesses unique electronic properties that originate from its relativistic Dirac-cone band structure with electron-hole symmetry. Under high magnetic fields B, the energy spectrum splits into unequally spaced relativistic Landau levels (LLs) with energies $\propto \sqrt{B|N|}$, where N (= $0, \pm 1, \pm 2, \dots$) is the Landau orbital index. However, its most salient feature is the existence of the zero-energy LL with $N = 0$, equally shared by electronlike and holelike states, which is responsible for the distinctive half-integer quantum Hall (QH) effect [1,2] and is the hallmark of the Dirac nature of charge carriers in graphene.

A further interesting feature of Dirac electrons in graphene is brought about by the existence of two equivalent sublattices in its honeycomb structure, which couple with the orbital motion to form two Dirac cones located at K and K' points in the momentum space. The sublattice pseudospin, which encodes the amplitude of the wave function on the two sublattices, is locked with the direction of motion, making the chirality a good quantum number [3–5]. In the zero-energy LL, the chirality is directly related to the sublattice symmetry, which can make the $N = 0$ LL behave differently from other LLs in the presence of disorder. Theory predicts that, when disorder preserves the chiral symmetry in the zero-energy states, the zeroth LL is protected from the broadening due to disorder. The types of such disorder include bond disorder [6] and hopping disorder with a correlation length of several tens of nanometers, which can be induced by ripples in graphene [7,8]. On the other hand, when the type of disorder is such that the chiral symmetry is broken, as in a random potential, the zeroth and first LLs are expected to be subject to broadening of a similar magnitude [9,10].

In this paper we report on our measurements of the disorder broadening of LLs in epitaxial graphene on SiC. Specifically, we examine the behavior of the zeroth and first LLs to characterize the type of disorder present in epitaxial graphene. We employ two different methods for the same sample, namely gated transport spectroscopy and activation gap measurements on the QH states. As reported in Ref. [11], gated transport spectroscopy works in the presence of nearby interface states with a known density of states (DOS), which provide the conversion from gate voltage to the Fermi level. The method allows the direct probing of the extended-state width, which was demonstrated at 1.5 K in Ref. [11]. Here we systematically investigate the temperature dependence of the extended-state width. Under certain assumptions we find a power-law temperature dependence with the exponent $\eta \sim 0.3$ for both the zeroth and first LLs. The obtained extended-state widths are then compared with those deduced from the activation gap measurements. While the transport spectroscopy shows similar width for the zeroth and first LLs, the activation measurements indicate a larger broadening of the zeroth LL. These results indicate that random disorder [9] is dominant in our epitaxial graphene sample, rather than the typical hopping disorder caused by ripples [7].

This paper is organized as follows. Section II describes the sample fabrication and measurement methods. Section III presents the transport spectroscopy. Section IV presents activation gap measurements performed on the same sample. In Sec. V the results obtained from the two methods are compared and discussed. Our results obtained from epitaxial graphene with adjacent interface states are compared with previous reports on various graphene samples including exfoliated graphene on SiO$_2$. The last section provides a summary.

II. SAMPLE AND METHOD

Our device is a top-gated Hall bar 200 μm long and 40 μm wide, fabricated from graphene epitaxially grown on 6H-SiC(0001). The graphene growth procedure is similar to that reported in Ref. [12]. We chemically cleaned the SiC surface, heated the SiC wafer in a furnace to around 2000 K in an Ar atmosphere ($\leqslant$100 torr), and then cooled it to room temperature. The whole surface was then covered with continuous regions of monolayers of graphene and discontinuous narrow strips consisting of unintentionally grown few-layer graphene. Since few-layer graphene is formed

---
[*]takase.keiko@lab.ntt.co.jp
[†]Present address: Graduate School of Science and Technology, Kwansei Gakuin University, Sanda, Hyogo 669-1337, Japan.

as flakes or islands less than several micrometers in size, the charge transport measurements probe only the properties of monolayer graphene in high magnetic fields [11]. Under this growth condition, a $6\sqrt{3} \times 6\sqrt{3}$ buffer layer with dangling-bond states emerges under the monolayer graphene [11,13–15].

On the graphene/SiC wafer, HSQ was deposited followed by sputtered SiO_2. The SiO_2/HSQ gate insulator made with the above method does not degrade the carrier mobility in graphene, similarly to the polymer [15,16] or dielectrics with high permittivity [17].

Transport measurements were performed using standard lock-in techniques with a current of ~10 nA at temperatures of 1.6 to 150 K. We examined several devices and confirmed that similar results are generally produced. For the quantitative consistency of our analysis, we here present the results obtained from one sample.

III. GATED TRANSPORT SPECTROSCOPY

A. Gate-voltage dependence of Fermi level

To explain how our transport spectroscopy works, we first illustrate the impact of interface states near graphene on the relation between gate voltage V_g and the Fermi level ε_F of graphene. Figure 1(a) shows a two-dimensional plot of the longitudinal resistance R_{xx} at 1.6 K as a function of V_g and B. Integer QH states at a LL filling factor $\nu \equiv n_G h/eB$ of ± 2, $+6$, and $+10$ are visible as dark regions separated by R_{xx} peaks at $\nu = 0$, 4, and 8. (n_G is the electron density in graphene, h is Planck's constant, and e is the elementary charge.) The striking feature of the data in Fig. 1(a) is that the Landau fan appears as a set of unequally spaced parabolic curves, instead of equally spaced straight lines as usually observed in graphene as well as in conventional semiconductors. The similarity between the trajectories of the R_{xx} peaks in Fig. 1(a) and the energy diagram of the relativistic graphene LLs is obvious if we take the V_g axis in Fig. 1(a) as the energy axis. This indicates that the unusual relation $\varepsilon_F \propto V_g - V_{CNP}$ holds in our sample, as opposed to the normal behavior $n_G \propto V_g - V_{CNP}$, where V_{CNP} is the gate voltage at the charge neutrality point.

As shown in Ref. [11], this unusual behavior is due to the interplay between graphene quantum capacitance and interface state density of states (DOS). Figure 1(b) illustrates the essence of the model. When V_g is varied, charge redistribution occurs among the top gate, graphene, and the interface states immediately below and above the graphene with a constant DOS γ_1 and γ_2, respectively [18]. When the DOS of the interface states is large as compared to that of the graphene LLs, most of the gate-induced charges are accommodated by the interface states. In this case, the Fermi level of graphene, which equals the electrochemical potentials of the interface states, moves almost linearly with V_g. Consequently, gate sweep measurements function as the energy spectroscopy of graphene LLs. The model in Ref. [11] allows us to calculate n_G and hence ν as a function of V_g and B. The curves of constant filling $\nu = 4N$ ($N = 0, \pm 1, \pm 2, \ldots$), calculated with appropriate values of γ_1 and γ_2, match the trajectories of the R_{xx} peaks, as shown by the dashed lines in Fig. 1(a). The solid lines in Fig. 1(a) delineate the borders between
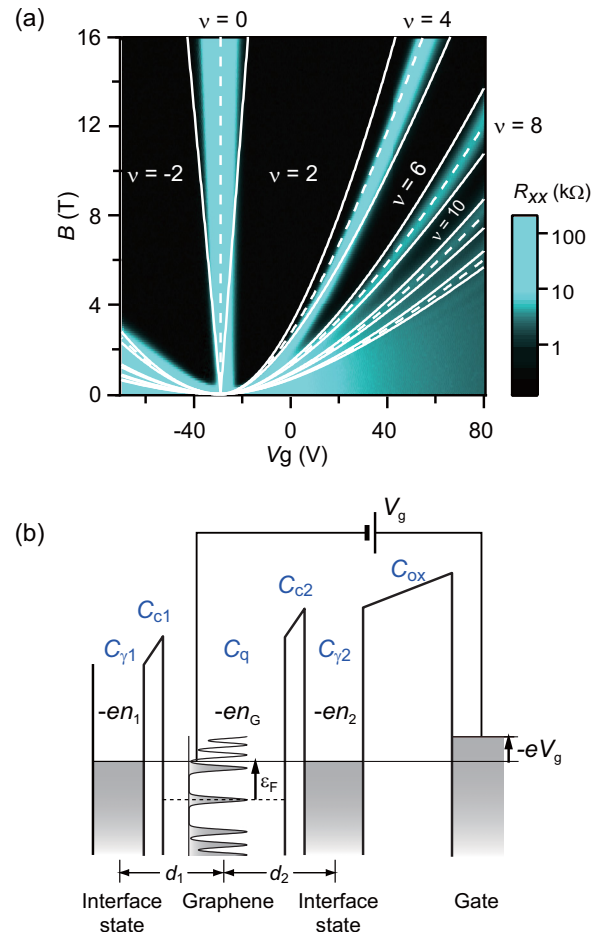
FIG. 1. (Color online) (a) R_{xx} plotted vs V_g and B measured at $T = 1.6$ K. The dashed and solid lines show the results of calculations using the model in (b). The dashed lines represent the half-fillings of the graphene LLs, i.e., $\nu = 4N$. The solid lines indicate borders separating regions with integer and noninteger fillings. (b) Schematic energy diagram of graphene and the interface states above and below graphene in the presence of magnetic fields. $-en_1$ and $-en_2$ are the charge densities of the interface states below and above graphene, respectively.

the regions where the Fermi level is in the gap between LLs and those where it lies in a LL. The width of the latter regions, which we denote by ΔV_ϕ, represents the change in V_g necessary to fill an empty LL in the absence of disorder.

Our aim is to deduce the width ΔE of the extended states from the measured width ΔV_g of the R_{xx} peaks. There are two contributors to ΔV_g with different physical origins: one is associated with the transfer of charge from the gate to the graphene (and interface states), and the other with the shift of the Fermi level by ΔE. The former can be expressed as $(\Delta n_G/n_\phi)\Delta V_\phi$, where $n_\phi \equiv 4eB/h$ is the LL degeneracy and Δn_G is the change in carrier density that occurs when the gate voltage is varied by ΔV_g. Thus, ΔE can be expressed as [19]

$$\Delta E = \beta e \left(\Delta V_g - \frac{\Delta n_G}{n_\phi} \Delta V_\phi \right), \qquad (1)$$

where

$$\beta = \frac{C_{\text{ox}}}{C_{\text{s1}} + C_{\text{s2}}}\left(1 + \frac{C_{\gamma 2}}{C_{\text{c2}}}\right)^{-1} \qquad (2)$$

is a dimensionless constant and

$$\Delta V_\phi = \left(1 + \frac{C_{\gamma 2}}{C_{\text{c2}}}\right)\frac{en_\phi}{C_{\text{ox}}}. \qquad (3)$$

(See Appendix for a more detailed derivation of these equations and the parameters used in this paper.) In Eqs. (2) and (3) C_{ox} is the capacitance of the gate insulator, C_{ci} is the geometrical capacitance between graphene and the interface states, $C_{\gamma i} \equiv e^2 \gamma_i$ is the quantum capacitance [20] of the interface states, and $C_{\text{si}} = (1/C_{\text{ci}} + 1/C_{\gamma i})^{-1}$, where the subscript $i = 2$ (1) refers to the upper (lower) interface states. (Throughout this paper we use the term "capacitance" to refer to the capacitance per unit area.) In the next subsection we use Eq. (1) to deduce ΔE from ΔV_{g} measured at different temperatures.

B. Experimental estimation of LL broadening

Figure 2 shows the traces of R_{xx} vs V_{g} (black solid lines) at $B = 4$, 10, and 16 T, taken at $T = 1.6$ K. At a high B, the R_{xx} peaks at $\nu = 0$ and 4 are well separated from the others. As shown by the dashed lines, these peaks can be nicely fitted with Gaussian functions, from which we deduce the full width at half maximum ΔV_{g}. We fitted the R_{xx} traces obtained at different temperatures ranging from 1.6 to 150 K to deduce ΔV_{g} for the $N = 0$ and $N = 1$ LLs. At an elevated T, R_{xx} peaks become broader and adjacent peaks start to overlap. Such an overlap between LLs becomes particularly relevant at low fields and for high LLs, where the LL energy separation becomes small. In such cases, peak decomposition was carried
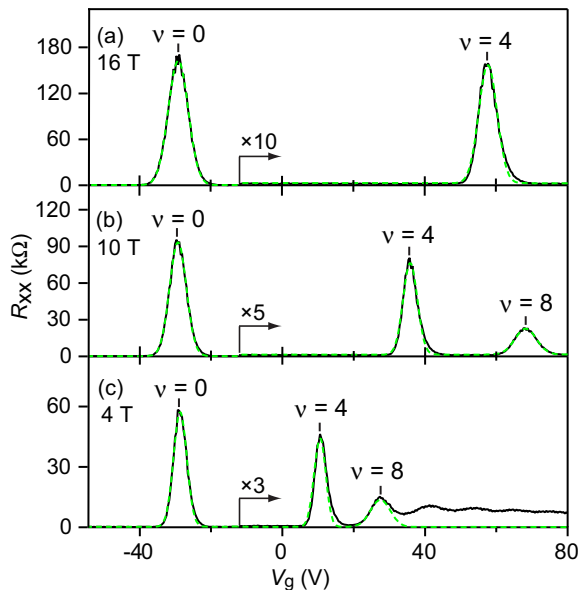
FIG. 2. (Color online) R_{xx} as a function of V_{g} at magnetic fields of (a) 16, (b) 10, and (c) 4 T. The solid lines indicate experimental data. The dashed lines are fits to the data with Gaussian functions. In (c), only the R_{xx} peaks corresponding to the $N \leqslant 2$ LLs are fitted.
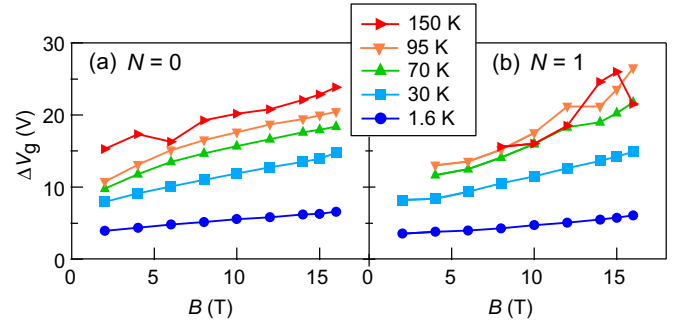
FIG. 3. (Color online) Width ΔV_{g} of the R_{xx} peaks in the (a) $N = 0$ and (b) $N = 1$ LLs at various T, plotted as a function of B.

out using multiple Gaussian functions to extract the ΔV_{g} value for each LL (see the $B = 4$ T data in Fig. 2). In the following analysis we use only those data with the maximum overlap occurring at tails lower than $\sim 10\%$ of the peaks.

In Figs. 3(a) and 3(b) the ΔV_{g} values deduced for the $N = 0$ and 1 LLs at different temperatures are plotted as a function of B, respectively. The $N = 0$ and 1 LLs share a similar dependence of ΔV_{g} on B and T. ΔV_{g} is an increasing function of both B and T, with the B dependence becoming stronger at higher T. We attribute the observed T dependence of ΔV_{g} to the increased fraction of the extended states at elevated temperatures. This is reasonable, as the overall LL width including both the extended and localized states is determined mostly by a sample-dependent static disorder.

We assume that the disorder broadening of each LL is described by a Gaussian-shaped DOS

$$D(E) \equiv \frac{n_\phi}{\sqrt{2\pi}\sigma} \exp\left[-\frac{(E - \varepsilon_{\text{c}})^2}{2\sigma^2}\right], \qquad (4)$$

with the full width at half maximum $W = 2\sqrt{2\ln 2}\sigma$ (σ is the standard deviation of the DOS) and the level center ε_{c}. Then, Δn_{G} and ΔE in Eq. (1) are linked to each other as

$$\Delta n_{\text{G}} = \int D(E)[f(E, \varepsilon_{\text{c}} + \Delta E/2) - f(E, \varepsilon_{\text{c}} - \Delta E/2)]dE, \qquad (5)$$

where $f(E, \mu) \equiv 1/[1 + e^{(E-\mu)/k_{\text{B}}T}]$ is the Fermi-Dirac function (k_{B} is the Boltzmann constant) [21]. Thus, ΔE can be obtained by solving Eqs. (1) and (5) self-consistently. Note that Eq. (5) includes finite-temperature effects, allowing us to estimate ΔE over a broad temperature range. To analyze the experimental data, we introduce a dimensionless parameter $r \equiv \Delta E/W$ and use r, instead of W, as an input parameter. We take $r = 0.5$ at $T = 95$ K independent of B. As we will see later, this yields results consistent with the activation gap measurements [22]. ΔE obtained in this way is used to deduce $W (= \Delta E/r)$ at each B, and this W value is used to analyze the data at different temperatures.

The results for the data at $B = 8$, 12, and 15 T are compiled in Figs. 4(a) and 4(b), where ΔE for the $N = 0$ and $N = 1$ LLs is plotted as a function of T, respectively. In the following we denote the extended-state width of the Nth LL by ΔE_N^{sp}. (The superscript indicates experimental values deduced from transport spectroscopy.) We find that ΔE_0^{sp} is
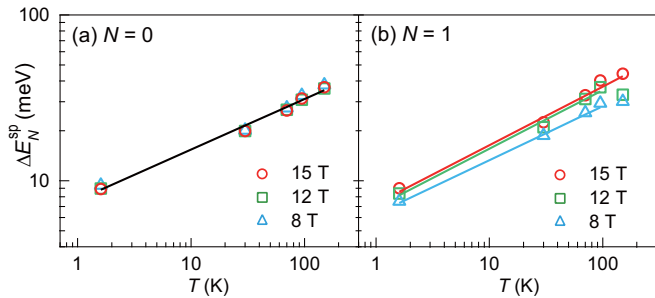
FIG. 4. (Color online) T dependence of ΔE_N^{sp} at different B deduced for the (a) $N = 0$ and (b) $N = 1$ LLs. The solid lines represent power-law fits, $\Delta E_N^{sp} \propto T^\eta$, yielding $\eta = 0.30$–0.31 for $N = 0$ and $\eta = 0.32$–0.35 for $N = 1$.

nearly B independent; the data for different magnetic fields collapse onto a single line in the log-log plot, indicating the power-law behavior given by $\Delta E_0^{sp} \propto T^\eta$ with $\eta = 0.30$–0.31. On the other hand, ΔE_1^{sp} shows a slight increase with B. Yet, the temperature dependence of all the data fits nicely with the power law with $\eta = 0.32$–0.35, except for those at the highest T of 150 K [23].

It is interesting to compare the exponent η deduced above and the critical exponent κ of the QH plateau-to-plateau transition. By performing magnetoconductivity measurements on an exfoliated graphene sample, Giesbers *et al.* found a power-law dependence with $\kappa = 0.37 \pm 0.05$ for the width of $d\sigma_{xx}/d\nu$ and $\kappa = 0.41 \pm 0.04$ for $d\sigma_{xy}/d\nu$ in the $N = 1$ LL, where σ_{xx} and σ_{xy} are diagonal and Hall conductivities, respectively. In contrast, they observed essentially no temperature dependence in the $N = 0$ LL [24]. (On the other hand, using an exfoliated sample with an insulating behavior at $\nu = 0$, Amado *et al.* obtained $\kappa = 0.58 \pm 0.03$ for the plateau-insulator transition in the $N = 0$ LL [25].) A more recent study by Shen *et al.* of epitaxial graphene samples found $\kappa \sim 0.42$ for the $N = 1$ LL [26], while the $N = 0$ LL was not accessed in their top-gated epitaxial graphene. These values reported for the $N = 1$ LL in graphene are consistent with the value $\kappa \sim 0.42$ known for conventional two-dimensional systems with short-range disorder [27–29]. Considering the difference in the way η and κ are defined and deduced, the similarity between the values, $\eta = 0.32$–0.35 and $\kappa \sim 0.42$, is noteworthy. However, we will not attempt a more quantitative comparison as our analysis is based on many assumptions. Nevertheless, our data clearly demonstrate that in our epitaxial graphene device the $N = 0$ and $N = 1$ LLs behave similarly, both qualitatively and quantitatively.

IV. ACTIVATION GAP MEASUREMENTS

Activation gap measurements of QH states have often been used to estimate the width of disorder-broadened LLs [30,31]. When the Fermi level is located in the middle of a gap between adjacent LLs, the thermal excitation of charge carriers across the LL gap gives rise to finite bulk transport at elevated temperatures. The temperature dependence of the longitudinal resistance is described by the Arrhenius relation $R_{xx} \propto \exp(-\Delta/2k_B T)$, where Δ is the activation gap. In the absence of disorder, and if the contribution of Coulomb interaction
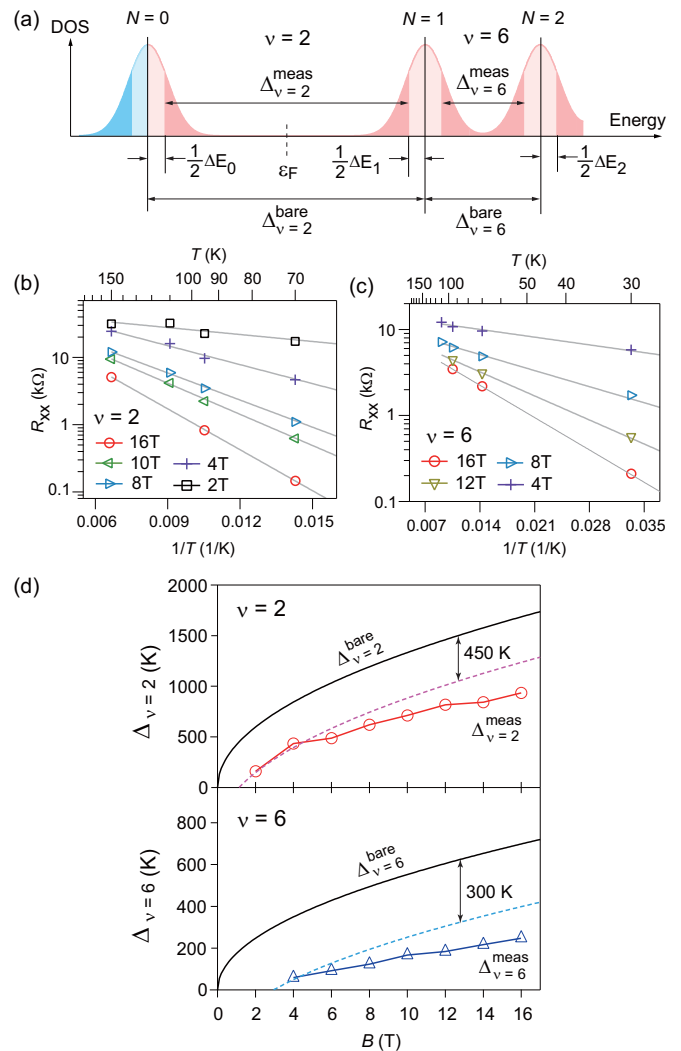
FIG. 5. (Color online) (a) Sketch of the DOS of disorder-broadened graphene LLs. Extended and localized states are shown in bright and dark colors, respectively. (b) and (c) R_{xx} as a function of $1/T$ at (b) $\nu = 2$ and (c) $\nu = 6$, measured at different B. The solid lines are fits to the data using the Arrhenius relation. (d) $\Delta_{\nu=2}$ (top) and $\Delta_{\nu=6}$ (bottom) vs B. $\Delta_{\nu=2(6)}^{meas}$, indicated by open symbols, is the measured activation gap at $\nu = 2(6)$, while $\Delta_{\nu=2(6)}^{bare}$ is the energy spacing between the relevant LLs. The dashed lines represent the behavior expected for a constant gap reduction of 450 (300) K from $\Delta_{\nu=2(6)}^{bare}$.

is negligible, Δ would equal the LL separation, which we denote by Δ^{bare}. Experimentally, however, the measured gaps Δ^{meas} are usually smaller than the LL separation, and their difference $\Gamma = \Delta^{bare} - \Delta^{meas}$ is attributed to the finite width of the LLs. It is generally understood that Δ^{meas} measures the energy difference between the lower end of the extended states in the upper LL and the upper end of the extended states in the lower LL [Fig. 5(a)]. The width ΔE_N of the extended states in the Nth LL can thus be deduced from the activation gaps at $\nu = 4N + 2$ using the following relation:

$$\Delta_{\nu=4N+2}^{meas} = \Delta_{\nu=4N+2}^{bare} - \frac{1}{2}(\Delta E_N + \Delta E_{N+1}), \quad (6)$$

where $\Delta_{\nu=4N+2}^{bare} = \nu\sqrt{2\hbar eB}(\sqrt{N+1} - \sqrt{N})$ with ν the Fermi velocity [32] and $\hbar = h/2\pi$.

We performed activation gap measurements of the QH states at $\nu = 2$ and 6 to estimate ΔE_0 and ΔE_1. Figures 5(b) and 5(c) show the Arrhenius plots of R_{xx} at $\nu = 2$ and 6, respectively, measured at various magnetic fields. As the solid lines indicate, R_{xx} vs $1/T$ can be fitted with $R_{xx} \propto \exp(-\Delta_\nu^{\mathrm{meas}}/2k_B T)$ over the temperature ranges shown. The values of $\Delta_{\nu=2}^{\mathrm{meas}}$ and $\Delta_{\nu=6}^{\mathrm{meas}}$ obtained from these fits are plotted as a function of B in Fig. 5(d). The plots show that for both $\nu = 2$ and 6, the measured gap is significantly smaller than the energy separation $\Delta_\nu^{\mathrm{bare}}$ between the relevant LLs. As shown in the figure, a gap reduction by $\Gamma = 450$ K for $\nu = 2$ (300 K for $\nu = 6$) accounts for the measured gap at low fields ($\leqslant 4$ T). However, if we assume that Γ is constant and B independent, at high fields we obtain $\Delta_\nu^{\mathrm{meas}}$ values that are considerably larger than those observed. This suggests that Γ is an increasing function of B.

V. DISCUSSION

We estimate the width of the extended states in the $N = 0$ and 1 LLs from the measured activation gaps at $\nu = 2$ and 6. An important assumption we used is that the broadening of the $N = 2$ LL is identical to that of the $N = 1$ LL. This assumption is reasonable as the $N \neq 0$ LLs are not affected by the presence of the particle/hole symmetry or the chiral symmetry in graphene. It is also partially verified by the transport data, which indicate similar ΔV_g values for the $N = 1$ and $N = 2$ LLs. Hence, substituting $\Delta E_2 = \Delta E_1$ into Eq. (6) with $N = 1$, we obtain ΔE_1 from $\Delta_{\nu=6}^{\mathrm{meas}}$. Then, using this ΔE_1 value along with Eq. (6) with $N = 0$, we obtain ΔE_0 from $\Delta_{\nu=2}^{\mathrm{meas}}$.

The open circles in Figs. 6(a) and 6(b) represent the obtained ΔE_0^{ac} and ΔE_1^{ac}, respectively, plotted as a function of B. (The superscript of ΔE_N^{ac} indicates experimental values deduced from the activation gap measurements.) For comparison, ΔE_0^{sp} and ΔE_1^{sp} obtained from transport spectroscopy at 95 K are plotted together by filled triangles. The temperature of 95 K was chosen so that it overlaps the temperature range of the activation measurements. Note that ΔE_0^{sp} and ΔE_1^{sp} are calculated with $r = 0.5$. This r value was chosen because it gives ΔE_1^{sp} consistent with ΔE_1^{ac} over the entire range of magnetic fields.

In contrast to the $N = 1$ LL, for which the transport spectroscopy and activation measurements give consistent results, for the $N = 0$ LL, the two methods give different results: ΔE_0^{ac} is much larger than ΔE_0^{sp}. Consequently, the activation measurements indicate that ΔE_0^{ac} is more than twice as large as ΔE_1^{ac}, whereas the transport spectroscopy indicates $\Delta E_0^{\mathrm{sp}} \sim \Delta E_1^{\mathrm{sp}}$. Nevertheless, it is fair to say that we found no evidence that the $N = 0$ LL is narrower than the $N = 1$ LL in either experiment. This indicates that random disorder [9,10] is dominant in our sample, rather than the oriented-hopping disorder that preserves the chiral symmetry [7,8].

The origin of the disagreement between the results of the two experiments for the $N = 0$ LL is unclear at present. If we consider the fact that transport spectroscopy seems to probe the extended-state width more directly [33], the disagreement is likely to be due to the overestimation of ΔE_0^{ac} or $\Gamma = \Delta^{\mathrm{bare}} - \Delta^{\mathrm{meas}}$. As shown in Fig. 5(d), for $\nu = 2$ and 6, Γ grows with increasing B. This behavior is qualitatively
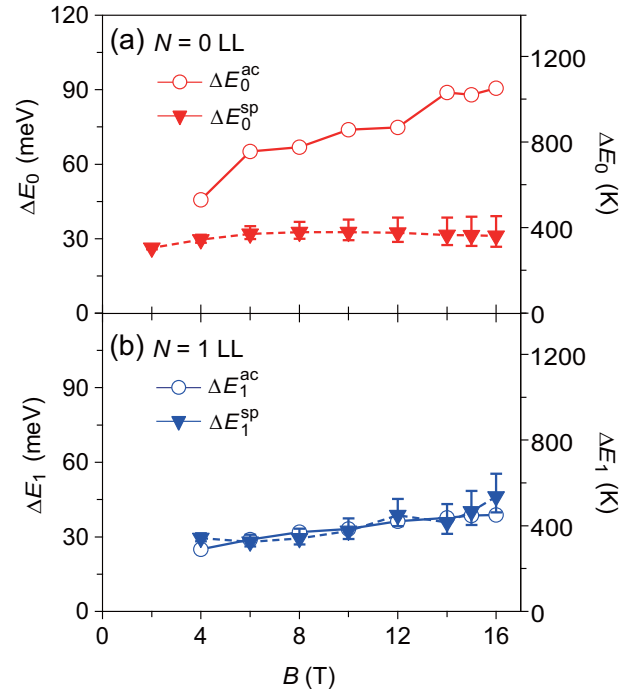
FIG. 6. (Color online) ΔE_N^{ac} (open circles) as a function of B for (a) $N = 0$ and (b) $N = 1$. For comparison, ΔE_N^{sp} at 95 K (closed triangles) deduced with $r = 0.5$ are shown. The error bars indicate the range of values that ΔE_N^{sp} takes when r is varied from 0.3 to 0.7.

different from that in previous reports, where Γ is nearly B independent [34], or decreases with increasing B [31,35]. Γ increasing with B was reported for bilayer graphene on SiO_2 [30], where the B dependence was attributed to the inhomogeneous perpendicular component of B that could be induced by ripples [36–38] in graphene. However, such a scenario seems unrealistic for the present case. To account for both the large Γ value and its B dependence, the ripple angles must be as large as $\sim 30°$ with respect to the sample normal [39]. This is much larger than the typical ripple angle of a few degrees in epitaxial graphene [36]. In addition, such large ripple angles would imply that the perpendicular B component ranges from 1.0 to 0.87 times that of the applied B. In such a situation the $\nu = 10$ QH state would hardly be resolved.

Finally, we refer to previous studies on different types of graphene samples using various experimental approaches [31,35,40–44]. Scanning tunneling microscopy performed on graphene on graphite at 4 K showed that the width of the zeroth LL (~ 25 meV) was slightly larger than that of higher LLs (~ 15 meV) [40]. Transport measurements on double layers of graphene separated by a thin dielectric layer produced very similar results, namely 28 and 13 meV for the zeroth and first LLs, respectively [41,42]. Capacitance measurements on graphene on SiO_2 revealed broadening of a similar magnitude (30 meV) for the zeroth and first LLs [43]. In contrast, activation gap measurements performed for graphene on SiO_2/Si at a very high magnetic field of 30 T revealed different behavior [31,35]. The measurements show that, while the broadening of the extended states in the first LL was around 35 meV, that of the zeroth LL was vanishingly small even at $T \geqslant 150$ K. As shown in Fig. 6, our transport spectroscopy

data at 95 K analyzed with $r = 0.5$ yield $\Delta E \sim 30$ meV for both $N = 0$ and $N = 1$ LLs, which translates into the overall LL width of $W \sim 60$ meV. We emphasize that a direct comparison between our results and previous reports is difficult, as the interface states present in our epitaxial graphene sample may provide an additional scattering mechanism. Nevertheless, we believe that our results will stimulate further work to gain deeper understanding of the disorder effects in graphene and other types of two-dimensional electron systems.

Further studies are needed to explore the LL broadening in differently fabricated epitaxial graphene devices, such as those using a different gate insulator and a SiC substrate with a different orientation [45] or a substrate modulated by N doping [46,47].

VI. SUMMARY

In summary, we characterized the disorder broadening of LLs in top-gated epitaxial graphene using two independent methods applied to the same sample. Transport spectroscopy indicates that the widths of the extended states in the $N = 0$ and 1 LLs are similar both in magnitude and in their dependence on temperature and magnetic field. Activation measurements gave results consistent with transport spectroscopy for the $N = 1$ LL, but indicated a considerably larger broadening for the $N = 0$ LL. These results indicate that the random potential disorder is dominant in our epitaxial graphene.

ACKNOWLEDGMENTS

APPENDIX: DERIVATION OF EQUATIONS

In this Appendix we derive Eqs. (1)–(3) of the main text. Suppose that the Fermi level of graphene moves from ε_F to $\varepsilon_F + \delta\varepsilon_F$ within a disorder-broadened LL as the gate voltage is varied from V_g to $V_g + \delta V_g$. The resultant change δn_G in n_G is accompanied by additional charge transfers $-e\delta n_1$

and $-e\delta n_2$ from the gate to the lower and upper interface states, respectively, where the electrochemical equilibrium with graphene is given by

$$\delta n_1(1/\gamma_1 + e^2/C_{c1}) = \delta\varepsilon_F, \tag{A1}$$

$$\delta n_2/\gamma_2 - (\delta n_1 + \delta n_G)e^2/C_{c2} = \delta\varepsilon_F. \tag{A2}$$

Here the term $\delta n_{1(2)}/\gamma_{1(2)}$ represents the shift in the chemical potential of the lower (upper) interface states. The remainder on the left-hand sides represents the change in the electrostatic potential caused by the net charge transfer from the upper interface states to graphene $-e(\delta n_1 + \delta n_G)$ and that from graphene to the lower interface states $-e\delta n_1$. $C_{c1(2)} \equiv \varepsilon_{1(2)}/d_{1(2)}$ is the geometrical capacitance between graphene and the lower (upper) interface states, where $d_{1(2)}$ and $\varepsilon_{1(2)}$ are the relevant distance and effective permittivity. By substituting these equations into $e(\delta n_1 + \delta n_2 + \delta n_G) = C_{ox}\delta V_g$, where C_{ox} is the capacitance of the gate insulator, we have

$$\delta n_G + \frac{C_{s1} + C_{s2}}{e^2}\delta\varepsilon_F = \frac{C_{ox}}{e}\left(1 + \frac{C_{\gamma 2}}{C_{c2}}\right)^{-1}\delta V_g. \tag{A3}$$

Here $C_{\gamma 1(2)} \equiv e^2\gamma_{1(2)}$ is the quantum capacitance [20] of the lower (upper) interface states, and $C_{s1(2)} \equiv [1/C_{\gamma 1(2)} + 1/C_{c1(2)}]^{-1}$.

The change in V_g necessary to fill an empty LL in the absence of disorder is obtained by substituting $\delta\varepsilon_F = 0$, $\delta n_G = 4eB/h \ (\equiv n_\phi)$, and $\delta V_g = \Delta V_\phi$ into Eq. (A3) as

$$\Delta V_\phi = \left(1 + \frac{C_{\gamma 2}}{C_{c2}}\right)\frac{en_\phi}{C_{ox}}$$

[Eq. (3) of the main text]. The width ΔE of the extended state in the presence of disorder is obtained by substituting $\delta n_G = \Delta n_G$, $\delta\varepsilon_F = \Delta E$, and $\delta V_g = \Delta V_g$ into Eq. (A3) as

$$\Delta E = \beta e\left(\Delta V_g - \frac{\Delta n_G}{n_\phi}\Delta V_\phi\right),$$

where

$$\beta = \frac{C_{ox}}{C_{s1} + C_{s2}}\left(1 + \frac{C_{\gamma 2}}{C_{c2}}\right)^{-1}$$

[Eqs. (1) and (2) of the main text]. For the analysis presented in this paper, we used $\gamma_1 = 5.0 \times 10^{12}$ eV^{-1} cm^{-2} [15], $\gamma_2 = 3.4 \times 10^{13}$ eV^{-1} cm^{-2}, $d_1 = d_2 = 0.3$ nm, $\varepsilon_1 = \varepsilon_0$, and $\varepsilon_2 = 3\varepsilon_0$, where ε_0 is the vacuum permittivity. These parameters yield $\beta = 0.0027$.

[1] K. S. Novoselov, A. K. Geim, S. V. Morozov, D. Jiang, M. I. Katsnelson, I. V. Grigorieva, S. V. Dubonos, and A. A. Firsov, Nature (London) **438**, 197 (2005).

[2] Y. Zhang, Y. Tan, H. L. Stormer, and P. Kim, Nature (London) **438**, 201 (2005).

[3] A. K. Geim and K. S. Novoselov, Nat. Mater. **6**, 183 (2007).

[4] M. I. Katsnelson, Mater. Today **10**, 20 (2007).

[5] M. I. Katsnelson and K. S. Novoselov, Solid State Commun. **143**, 3 (2007).

[6] A. H. Castro Neto, F. Guinea, N. M. R. Peres, K. S. Novoselov, and A. K. Geim, Rev. Mod. Phys. **81**, 109 (2009).

[7] T. Kawarabayashi, Y. Hatsugai, and H. Aoki, Phys. Rev. Lett. **103**, 156804 (2009).

[8] A. L. C. Pereira, C. H. Lewenkopf, and E. R. Mucciolo, Phys. Rev. B **84**, 165406 (2011).

[9] W. Zhu, Q. W. Shi, X. R. Wang, J. Chen, J. L. Yang, and J. G. Hou, Phys. Rev. Lett. **102**, 056803 (2009).

[10] K. Nomura and A. H. MacDonald, Phys. Rev. Lett. **96**, 256602 (2006).

[11] K. Takase, S. Tanabe, S. Sasaki, H. Hibino, and K. Muraki, Phys. Rev. B **86**, 165435 (2012).

[12] K. V. Emtsev, A. Bostwick, K. Horn, J. Jobst, G. L. Kellogg, L. Ley, J. L. McChesney, T. Ohta, S. A. Reshanov, J. Rohrl, E. Rotenberg, A. K. Schmid, D. Waldmann, H. B. Weber, and Th. Seyller, Nat. Mater. **8**, 203 (2009).

[13] F. Varchon, R. Feng, J. Hass, X. Li, B. N. Nguyen, C. Naud, P. Mallet, J.-Y. Veuillen, C. Berger, E. H. Conrad, and L. Magaud, Phys. Rev. Lett. **99**, 126805 (2007).

[14] S. Kopylov, A. Tzalenchuk, S. Kubatkin, and V. I. Fal'ko, Appl. Phys. Lett. **97**, 112109 (2010).

[15] T. J. B. M. Janssen, A. Tzalenchuk, R. Yakimova, S. Kubatkin, S. Lara-Avila, S. Kopylov, and V. I. Fal'ko, Phys. Rev. B **83**, 233402 (2011).

[16] S. Lara-Avila, K. Moth-Poulsen, R. Yakimova, T. Bjornholm, V. Fal'ko, A. Tzalenchuk, and S. Kubatkin, Adv. Mater. **28**, 878 (2011).

[17] T. Shen, J. J. Gu, M. Xu, Y. Q. Wu, M. L. Bolen, M. A. Capano, L. W. Engel, and P. D. Ye, Appl. Phys. Lett. **95**, 172105 (2009).

[18] We assume that the interface states are in electrochemical equilibrium with graphene but they do not contribute to lateral charge transport.

[19] Note that $\Delta n_G/n_\phi$ in Eq. (1) represents the fraction of the extended states with respect to the whole LL DOS. In Ref. [11] this quantity was represented by an effective parameter f, which was allowed to be temperature dependent but without taking into account the thermal activation across the Fermi level. Here we extend the model to incorporate the effects of thermal distribution of carriers within a disorder-broadened LL.

[20] S. Luryi, Appl. Phys. Lett. **52**, 501 (1988).

[21] Equation (5) assumes that the extended states exist symmetrically around the LL center and overlap between adjacent LLs is negligible.

[22] This approach also has the advantage that it does not require explicit assumptions about the value of W or its dependence on B.

[23] We note that η depends only weakly on the choice of the r value at 95 K. Whereas ΔE varies by 30% for $r(95\,\text{K}) = 0.3$–0.7, η varies only by 10%.

[24] A. J. M. Giesbers, U. Zeitler, L. A. Ponomarenko, R. Yang, K. S. Novoselov, A. K. Geim, and J. C. Maan, Phys. Rev. B **80**, 241411(R) (2009).

[25] M. Amado, E. Diez, D. Lopez-Romero, F. Rossella, J. M. Caridad, F. Dionigi, V. Bellani, and D. K. Maude, New J. Phys. **12**, 053004 (2010).

[26] T. Shen, A. T. Neal, M. L. Bolen, J. J. Gu, L. W. Engel, M. A. Capano, and P. D. Ye, J. Appl. Phys. **111**, 013716 (2012).

[27] H. P. Wei, D. C. Tsui, M. A. Paalanen, and A. M. M. Pruisken, Phys. Rev. Lett. **61**, 1294 (1988).

[28] S. Koch, R. J. Haug, K. V. Klitzing, and K. Ploog, Phys. Rev. Lett. **67**, 883 (1991).

[29] W. Li, C. L. Vicente, J. S. Xia, W. Pan, D. C. Tsui, L. N. Pfeiffer, and K. W. West, Phys. Rev. Lett. **102**, 216801 (2009).

[30] E. V. Kurganova, A. J. M. Giesbers, R. V. Gorbachev, A. K. Geim, K. S. Novoselov, J. C. Maan, and U. Zeitler, Solid State Commun. **150**, 45 (2010).

[31] A. J. M. Giesbers, U. Zeitler, M. I. Katsnelson, L. A. Ponomarenko, T. M. Mohiuddin, and J. C. Maan, Phys. Rev. Lett. **99**, 206803 (2007).

[32] Throughout the paper we use $v = 1.0 \times 10^6$ m/s for calculations.

[33] In contrast to the activation measurements in which two LLs are involved, only one LL is involved in transport spectroscopy. For this reason we believe that the latter method probes the extended-state width more directly. We also note that the interface states playing the role of the spectrometer have nearly constant density of states. Therefore, the obtained spectrum can be seen to directly reflect the electronic states in graphene.

[34] D. A. Abanin, S. V. Morozov, L. A. Ponomarenko, R. V. Gorbachev, A. S. Mayorov, M. I. Katsnelson, K. Watanabe, T. Taniguchi, K. S. Novoselov, L. S. Levitov, and A. K. Geim, Science **332**, 328 (2011).

[35] K. Bennaceur, P. Jacques, F. Portier, P. Roche, and D. C. Glattli, Phys. Rev. B **86**, 085433 (2012).

[36] F. Varchon, P. Mallet, J.-Y. Veuillen, and L. Magaud, Phys. Rev. B **77**, 235412 (2008).

[37] A. Deshpande, W. Bao, F. Miao, C. N. Lau, and B. J. LeRoy, Phys. Rev. B **79**, 205411 (2009).

[38] V. Geringer, M. Liebmann, T. Echtermeyer, S. Runte, M. Schmidt, R. Rückamp, M. C. Lemme, and M. Morgenstern, Phys. Rev. Lett. **102**, 076102 (2009).

[39] See the calculation method in A. J. M. Giesbers, Ph.D. thesis, Radboud University Nijmegen, 2010.

[40] G. Li, A. Luican, and E. Y. Andrei, Phys. Rev. Lett. **102**, 176804 (2009).

[41] S. Kim, I. Jo, D. C. Dillen, D. A. Ferrer, B. Fallahazad, Z. Yao, S. K. Banerjee, and E. Tutuc, Phys. Rev. Lett. **108**, 116404 (2012).

[42] S. Kim and E. Tutuc, Solid State Commun. **152**, 1283 (2012).

[43] L. A. Ponomarenko, R. Yang, R. V. Gorbachev, P. Blake, A. S. Mayorov, K. S. Novoselov, M. I. Katsnelson, and A. K. Geim, Phys. Rev. Lett. **105**, 136801 (2010).

[44] Z. Jiang, E. A. Henriksen, L. C. Tung, Y.-J. Wang, M. E. Schwartz, M. Y. Han, P. Kim, and H. L. Stormer, Phys. Rev. Lett. **98**, 197403 (2007).

[45] J. L. Xia, F. Chen, J. L. Tedesco, D. K. Gaskill, R. L. Myers-Ward, C. R. Eddy, D. K. Ferry, and N. J. Tao, Appl. Phys. Lett. **96**, 162101 (2010).

[46] D. Waldmann, J. Jobst, F. Speck, T. Seyller, M. Krieger, and H. B. Weber, Nat. Mater. **10**, 357 (2011).

[47] B. Jouault, N. Camara, B. Jabakhanji, A. Caboni, C. Consejo, P. Godignon, D. K. Maude, and J. Camassel, Appl. Phys. Lett. **100**, 052102 (2012).